

NASA TECHNICAL MEMORANDUM 100539

**SIMULATED IMPACT DAMAGE IN A THICK
GRAPHITE/EPOXY LAMINATE USING
SPHERICAL INDENTERS**

C. C. Poe, Jr.

(NASA-TM-100539) SIMULATED IMPACT DAMAGE IN
A THICK GRAPHITE/EPOXY LAMINATE USING
SPHERICAL INDENTERS (NASA) 35 p CSCI 11D

N88-20363

Unclas
G3/24 0129549

JANUARY 1988



National Aeronautics and
Space Administration

Langley Research Center
Hampton, Virginia 23665

INTRODUCTION

NASA is developing light-weight filament-wound cases (FWC) for the solid rocket motors of the Space Shuttle. They are made of graphite/epoxy using a wet filament-winding process. Each 3.66-m-diameter (12-ft) motor consists of four cases -- a forward case, two center cases, and an aft case -- that are joined to steel rings with pins. The forward and center cases are approximately 7.62 m (25 ft) in length, and the aft case is somewhat shorter. The FWC's are 3.6-cm (1.4-in.) thick except very near the ends where they are thicker to withstand the concentrated pin loads.

Tests [1-4] revealed that impacts by blunt objects with low velocity could reduce the uniaxial tension strength of the FWC laminate by as much as 37 percent without making visible surface damage. Sharp impacters caused visible surface damage but not much more strength loss than the blunt impacters. Radiographs and conventional ultrasonic attenuation maps did not even reveal the internal damage caused by the blunt impacters. However, when one of the specimens with nonvisible damage was deplied rather than pulled to failure, broken fibers were found in the outer layers directly beneath the impact site, explaining the loss of strength. The locus of broken fibers in each layer resembled a crack oriented normal to the direction of the fibers. Fiber damage of similar size was predicted using internal stresses calculated with Hertz's law and Love's solution for pressure applied on part of the boundary of a semi-infinite body. It was also predicted that damage initiates at a critical value of contact pressure and that the extent of the damage increases with increasing indenter diameter.

Those findings required further experimental verification. Accordingly, in the present investigation, numerous specimens with simulated impact damage were deplied to measure the extent of fiber damage in terms of contact pressure and indenter shape. A laminate that was cut from an actual FWC was used for this investigation. Impacts were simulated under quasi-static conditions by pressing hemispherically shaped indenters against the laminate at different locations. For a thick laminate and a given maximum force during impact, the damage caused by low-velocity impacts and these simulated impacts should not be significantly different. After the contact forces were applied, the laminate was cut into small squares, each containing a contact site, and deplied. No attempt was made to characterize the damage by conventional radiography because it was proven ineffective previously [1-4]. Also, this laminate was too porous (perhaps as much as 10 percent) to use ultrasonic attenuation. The size of damage was also predicted with the analysis. The deply experiments did indeed verify the predictions. The results are presented here.

Original measurements were made in English units and converted to SI units.

SYMBOLS

A_{11}, A_{22}, A_{12} Constants in Hertz equation, Pa (psi)
 E_i Young's moduli of indenter, Pa (psi)

E_{22}	Young's moduli of FWC layers normal to fiber direction, Pa (psi)
E_x, E_y	Young's moduli of FWC laminate, Pa (psi)
E_r, E_z	Young's moduli of transversely isotropic semi-infinite body or target, Pa (psi)
G_{12}	Shear modulus of FWC layers, Pa (psi)
G_{xy}	Shear modulus of FWC laminate, Pa (psi)
G_{zr}	Shear modulus of transversely isotropic semi-infinite body or target, Pa (psi)
k_i, k_t	factors in the Hertz law, Pa^{-1} (psi) ⁻¹
n_o	factor in the Hertz law, Pa (psi)
$p(\rho)$	contact pressure distribution, Pa (psi)
p_c	average contact pressure, Pa (psi)
P	contact force, N (lbf)
r_c	contact radius, m (in.)
R_i	radius of indenter, m (in.)
S_1	principal shear stress, Pa (psi)
S_{max}	maximum shear stress, Pa (psi)
S_u	shear strength, Pa (psi)
u	indentation or displacement, m (in.)
ρ	ratio r/r_c
ν_{xy}, ν_{yx}	Poisson's ratios of FWC laminate
ν_r, ν_{rz}	Poisson's ratios of transversely isotropic semi-infinite body or target
ν_i	Poisson's ratio of indenter
ν_t	Poisson's ratio of isotropic semi-infinite body or target
ν_{12}	principal Poisson's ratio of FWC layers
σ	normal or shear stress, Pa (psi)
ζ	ratio z/r_c
ζ_o	value of ζ at $r = 0$ where S_1 is a maximum

Subscripts:

1,2	principal coordinates of the FWC layers (The 1-direction is the fiber direction.)
x,y	Cartesian coordinates (The x-direction is the axial direction of the cylinder or hoop direction of the FWC laminate.)
r, θ , z	cylindrical coordinates (The z-direction is normal to the laminate.)

MATERIAL

In previous impact investigations [1-4] of FWC's, a 0.76-m-diameter (30-in.) full-thickness cylinder was used to represent the region away from the ends. No material from the cylinder remained to be used in this investigation. Instead, a 30.5-by-30.5-cm (12-by-12-in.) piece of an actual FWC was used. The materials and the layup of the cylinder and the piece of FWC were as nearly the same as manufacturing considerations would allow. Both were wound by Hercules Inc. using a wet process and AS4W-12K graphite fiber and HBRF-55A epoxy resin except for the hoop layers of the cylinder, which were hand laid using prepreg tape. Also, this piece of FWC was from an early configuration that had two more inner hoop layers than the cylinder. The FWC piece was 3.68 cm (1.45 in.) thick. This particular FWC had been pressurized to the maximum expected operating pressure. The burst pressure of the FWC is greater than 1.4 times the maximum expected operating pressure. Thus, the case should not have sustained any damage that would have affected the results of this study. There was no visual evidence to the contrary. It is believed that results from this investigation and the previous investigations that used the cylinder can be compared, at least as far as the material is concerned.

From outside to inside, the layup of the laminate was $((\pm 33.5^\circ)_2/90^\circ / [(\pm 33.5^\circ)_2/90^\circ]_3 / [(\pm 33.5^\circ)_2/90^\circ]_7 / (\pm 33.5^\circ/90^\circ)_2 / \pm 33.5^\circ/90^\circ_4 / \pm 33.5^\circ/90^\circ_2 / (\pm 33.5^\circ)_2 /$ cloth), where the 90° layers are the hoops and the $\pm 33.5^\circ$ layers are the helicals. The underlined $\pm 33.5^\circ$ helical layers have about 1.6 times as many tows per in. of width as the other helical layers and are thus thicker in the same proportion. The cloth layer at the inner surface has an equal number of fibers in the warp and weave directions. The layup is balanced (equal numbers of $+33.5^\circ$ and -33.5° layers) but not symmetrical about the midplane. Most of the hoop layers are closer to the inner surface than the outer surface.

TEST APPARATUS AND PROCEDURE

A grid of lines spaced 3.8 cm (1.5 in.) apart was drawn on the laminate making 64 test squares. See figure 1. Hemispherically shaped indenters were pressed against the laminate at the center of the 36 interior squares. The size of the damage was less than half the width of the test squares. Thus, damage at one site should not have affected that at another. The exterior squares were not used because of a concern that the free edges would affect the internal stresses and hence the damage.

The contact forces were applied with a 500-kN closed-loop, servo-controlled, hydraulic testing machine operating in a load-control mode. The load was increased very slowly by turning a potentiometer. After reaching the desired maximum load, the load was decreased slowly to zero in the same manner. Load and displacement were recorded during each test. The laminate lay on a 36x46x5-cm (14x18x2-in.) aluminum platen, which had one flat surface and one curved surface that mated with the laminate. See figure 2. The aluminum platen

was fastened to a flat 25x64x10-cm (10x25x4-in.) steel platen that was fastened to the hydraulic actuator. The indenters were screwed into an aluminum rod, which was held firmly by steel "L" grips. The indenter was centered on the fixed aluminum platen, and the laminate was moved around to align the indenter with the center of a square. The load vector was always normal to the curved surface of the laminate. The hemispherical indenters were made of a hardened steel and had diameters of 1.27, 2.54, and 5.08 cm (0.50, 1.00, and 2.00 in.).

For the 2.54-cm-diameter (1.00-in.) indenter, it was found [2-4] that the impact-force threshold for nonvisible damage was about 75.2 kN (16.9 kips), which corresponded to an average contact pressure of 640 MPa (93 ksi). Contact forces were chosen for each of the three indenter diameters to give a range of average contact pressure from 64 to 116 percent of 640 MPa (93 ksi), focusing attention on the threshold for nonvisible damage.

After the contact forces were applied, the laminate was cut into squares as shown in figure 1 and deplied [5]. In the deply process, the squares were heated to 400°C (752°F) for 60 minutes to partially pyrolyze or burn away the epoxy matrix. Following pyrolysis, the laminate was a loose stack of graphite layers. The top layer of the stack was the side that was contacted by the indenter. The layers were removed by pressing a piece of double-back adhesive tape against the top layer in the stack and lifting up the layer. Upon removal, each layer was affixed to a sheet of paper using the other side of the adhesive tape. All measurements of crack length were made on the bottom side of the layers using an optical microscope with relatively low magnification. The key to seeing the damaged fibers was proper lighting. The method used here was to look along the fibers and to tilt the specimen or light source so that the light was highly reflected by the fibers.

RESULTS AND ANALYSIS

Hertz law

An excellent treatise on the contact problem for composite materials and its application to impact was given by Greszczuk [6]. The following development is taken from Greszczuk. For a semi-infinite body that is homogeneous and transversely isotropic, the local displacement or indentation is given by

$$u = R_i^{-1/3} \left(\frac{P}{n_o} \right)^{2/3} \quad (1)$$

where

$$n_o = \frac{4}{3\pi(k_i + k_t)} \quad (2)$$

$$k_i = \frac{1 - \nu_i^2}{\pi E_i}$$

$$k_t = \frac{\sqrt{A_{22}} [(\sqrt{A_{11}A_{22}} + G_{zr})^2 - (A_{12} + G_{zr})^2]^{1/2}}{2\pi\sqrt{G_{zr}}(A_{11}A_{22} - A_{12}^2)}$$

$$A_{11} = \frac{E_z}{1 - \frac{2\nu_{rz}^2 E_z}{(1 - \nu_r)E_r}}$$

$$A_{22} = \frac{(\frac{E_r}{E_z} - \nu_{rz}^2)A_{11}}{1 - \nu_r^2}$$

$$A_{12} = \frac{\nu_{rz}A_{11}}{1 - \nu_r}$$

and ν_i , E_i , and ν_r , ν_{rz} , E_r , E_z , and G_{zr} are the elastic constants of the isotropic sphere (indenter) and the transversely isotropic semi-infinite body (target), respectively, and R_i is the radius of the sphere.

The corresponding contact radius is given by

$$r_c = \left(\frac{PR_i}{n_o}\right)^{1/3} \quad (3)$$

and the pressure distribution on the surface is given by

$$p(\rho) = \frac{3}{2}p_c(1 - \rho^2)^{1/2} \quad (4)$$

where $\rho = r/r_c$ and

$$p_c = \frac{P}{\pi r_c^2} \quad (5)$$

is the average contact pressure. Thus, the pressure varies from a maximum of $3p_c/2$ at $\rho = 0$ to zero at $\rho = 1$. Substituting equation (5) into (3) and eliminating the contact radius gives

$$p_c = \frac{1}{\pi} \left(\frac{n_o}{R_i}\right)^{2/3} P^{1/3} \quad (6)$$

or eliminating the contact force and solving for contact radius r_c gives

$$r_c = \frac{\pi p_c R_i}{n_o} \quad (7)$$

The elastic constants of the FWC laminate were not known. Recall that a full-thickness cylinder [1-4] was made to represent the FWC laminate. The elastic constants of the cylinder, which should be representative of the FWC laminate, are

$$\begin{aligned} E_x &= 30.6 \text{ GPa (2.86 Msi)} \\ E_y &= 39.0 \text{ GPa (5.66 Msi)} \\ G_{xy} &= 19.7 \text{ GPa (2.86 Msi)} \\ \nu_{xy} &= 0.351 \\ \nu_{yx} &= 0.447 \end{aligned}$$

The pertinent elastic constants for the hoop layers are

$$\begin{aligned} E_{22} &= 6.39 \text{ GPa (0.927 Msi)} \\ \nu_{12} &= 0.275 \\ G_{12} &= 4.47 \text{ GPa (0.649 Msi)} \end{aligned}$$

and for the helical layers are

$$\begin{aligned} E_{22} &= 1.92 \text{ GPa (0.278 Msi)} \\ \nu_{12} &= 0.267 \\ G_{12} &= 4.28 \text{ GPa (0.621 Msi)} \end{aligned}$$

In order to represent the cylinder as a transversely isotropic laminate, it was assumed that

$$\begin{aligned} E_r &= (E_x + E_y)/2 \\ &= 34.8 \text{ GPa (5.05 Msi)} \\ E_z &= E_{22} \\ &= 4.15 \text{ GPa (0.603 Msi)} \\ \nu_r &= (\nu_{xy} + \nu_{yx})/2 \\ &= 0.399 \\ \nu_{rz} &= \nu_{12} \\ &= 0.271 \\ G_{zr} &= G_{12} \\ &= 4.38 \text{ GPa (0.635 Msi)} \end{aligned}$$

Values of E_{22} , ν_{12} , and G_{12} for the hoop and helical layers were averaged. Assuming that

$$E_i = 207 \text{ GPa (30 Msi)}$$

$$\nu_i = 0.3$$

for the steel indenter, equation (2) gives $n_o = 4.69$ GPa (680 ksi).

An increase in E_r of 10 percent results in an increase in n_o of 2 percent, whereas an increase in E_z of 10 percent results in an increase in n_o of 11 percent. Thus, n_o increases in proportion to E_z , but is relatively insensitive to E_r . This result is consistent with the finding for generally orthotropic materials [5] that n_o is relatively insensitive to the inplane fiber orientations.

The load-displacement curves for loading were also used to determine n_o . The load-displacement curves were higher on loading than on unloading. Tan and Sun [7] attributed this difference to a permanent indentation. A value of n_o was calculated with equation (1) for each test using the maximum load and displacement or the load and displacement at 80 percent of the estimated impact-force threshold for nonvisible damage, whichever was smaller. The data was restricted because equation (1) does not account for damage. The average of the n_o values was 4.52 GPa (656 ksi) and the coefficient of variation was 0.0984. This value of n_o is within 3 percent of the value calculated with equation (2). However, the agreement could be fortuitous because the values of E_{22} for the hoop and helical layers are so different that one cannot be confident in using the average value of E_{22} for E_z .

A value for n_o was also determined from impact tests of the special cylinder [2-4] with the 2.54-cm-diameter (1.00-in.) indenter. Values of n_o were calculated with equation (3) using measured values of contact diameter and impact force for each test except when visible craters were made. Contact diameters were much larger when visible craters were made. The average value of n_o was 3.98 GPa (577 ksi), which is only about 12 percent less than that determined from the load-displacement curves of the FWC laminate.

Table I gives the contact forces that were applied to the specimens in terms of contact pressures calculated with equation (6) and $n_o = 4.52$ GPa (656 ksi).

Fiber Damage

Some examples of cracked layers are shown in figures 3-5 for the three indenters and the same average contact pressure of 648 MPa (94.0 ksi). Only the outer layers are shown for brevity. (There were 76 layers in the laminate.) The specimen in figure 3 was tested with the 1.27-cm-diameter (0.50-in.) indenter. Broken fibers are visible in the outer four layers directly beneath the contact site; the locus of breaks in each layer resembles a crack. Layers 5

and below were not damaged. The cracks are basically normal to the direction of the fibers. The cracks are so numerous and dense in the outer two layers that the damage resembles a hole. The specimen in figure 4 was tested with the 2.54-cm-diameter (1.00-in.) indenter. The damage is visible in the outer seven layers. The cracks are longer than those in figure 3. Multiple cracks are visible, although difficult to see without magnification, in layers 2, 4, and 5. The specimen in figure 5 was tested with the 5.08-cm-diameter (2.00-in.) indenter. The damage is more extensive than that for the two smaller indenters. Cracks are visible in the outer 17 layers. Multiple cracks are visible in layers 1 through 10. In layers 1, 2, and 3 and layers 4 and 5, some cracks in adjoining layers are coincident and not normal to the fibers. This interaction of cracks was probably caused by exceptionally good adhesion between those particular layers.

Also, photomicrographs of a highly magnified crack are shown in figure 6. The crack was in layer 7 of the cylinder [1-4]; layers 8 and below were not damaged. This specimen was impacted with a 2.54-cm-diameter (1.00-in.) indenter, producing a contact force of 54.3 kN (12.2 kips). The photograph in figure 6(a) shows the entire crack, and the photograph in figure 6(b) shows a small portion of the crack at an even higher magnification. The fiber breaks in this impacted specimen resemble those caused by the simulated impact with the same indenter and similar contact force in figure 4.

The number and length of cracks were measured in each layer for 20 of the specimens. The contact force, maximum crack length, and maximum crack depth is recorded in Table II for each specimen.

The half-length of cracks in each layer is plotted in figure 7 for the three indenters and six values of contact pressure. As noted previously, crack length was measured on the bottom side of the layers. For simplicity in plotting the data, crack length was assumed to be constant through the thickness of a layer. When layers had more than one crack, the length of the longest crack was plotted. In general, the length and depth of the cracks increase with contact pressure and indenter diameter. Cracks were not found in any layers for the smallest contact pressure, 408 MPa (59.2 ksi). At a pressure of 648 MPa (94.0 ksi), the reported threshold for nonvisible damage [2-4], the fiber damage is extensive.

Private communication with Mr. Carl Madsen of Hercules Inc. who has also deplied a FWC laminate with impact damage revealed that crack length did vary through the thickness of layers. Since measurements were only made on the bottom side of each layer here, it is possible that the crack lengths varied through the thickness of the layers. However, the variation is believed to not have been large. At least, a crack was never observed on one side and not on the other.

For an average contact pressure of 742 MPa (108 ksi), tests were duplicated for the 2.54- and 5.08-cm-diameter (1.00- and 2.00-in.) indenters. The damage sizes are plotted in figure 8. The results for the duplicate tests are in good overall agreement.

Internal Stresses

Love's solution for stresses in a semi-infinite body produced by pressure on part of the boundary [8] was used to calculate the internal stresses in the FWC laminate. The pressure distribution is given by equation (4). The solution is for a homogeneous isotropic body. Even though the laminate is made of orthotropic layers, the results should at least be qualitative.

The maximum values of stress from Love's solution for $\nu_t = 0.3$ and their locations are shown in figure 9. Cylindrical coordinates are used with $\rho = r/r_c$ and $\zeta = z/r_c$. The stresses are symmetrical about the z axis, that is the stresses are independent of θ . The maximum tensile stress is $\sigma_{rr} = 0.2 p_c$ and occurs on the surface at the perimeter of the contact site. The maximum tensile stress beneath the contact site ($\rho = 0$) is $\sigma_{\theta\theta} = \sigma_{rr} = 0.00867 p_c$ and occurs at $\zeta = 2.25$. Recall that fiber damage initiated for p_c between 408 and 514 MPa (59.2 and 74.6 ksi). The corresponding maximum tensile stress beneath the contact site is between 3.5 and 4.5 MPa (513 and 647 psi). Even at the perimeter of the contact site the tensile stress is only between 81.6 and 103 MPa (11.8 and 14.9 ksi). Thus, the tensile stresses are not sufficient to break fibers.

The maximum compressive stresses in figure 9 occur on the surface at the center of the contact site. The largest of these is σ_{zz} , which is $1.5 p_c$. This stress is normal to the layers and is more of a matrix stress than a fiber stress. The σ_{rr} and $\sigma_{\theta\theta}$ components, which are in the plane of the fibers, have a value of $1.2 p_c$. Thus, on the surface, the values of σ_{rr} and $\sigma_{\theta\theta}$ corresponding to damage initiation are between 490 and 617 MPa (71.0 and 89.5 ksi). However, below the surface at $\rho = 0$ and $\zeta = 0.482$, where S_1 is a maximum, σ_{rr} and $\sigma_{\theta\theta}$ are only $0.287 p_c$ or between 117 and 148 MPa (17.0 and 21.4 ksi) when damage initiates. Therefore, the compressive σ_{rr} and $\sigma_{\theta\theta}$ stresses could have caused fiber damage at the surface but not very far below the surface.

The maximum value of the shear stress σ_{rz} in figure 9 is $0.321 p_c$ and is located at $\rho = 0.85$ and $\zeta = 0.35$. However, because of symmetry, σ_{rz} is zero at $\rho = 0$ where the fibers break. On the other hand, the maximum value of the principal shear stresses S_1 is $0.465 p_c$ and occurs at $\rho = 0$ and $\zeta = 0.482$. This stress is given by

$$S_1 = [(\sigma_{rr} - \sigma_{zz})^2/4 + \sigma_{rz}^2]^{1/2} \quad (8)$$

Previous reported values of S_1 are incorrect [1-4]; they should be multiplied by 0.75. The value of S_1 corresponding to damage initiation is between 190 and 239 MPa (27.5 and 34.6 ksi). For unidirectional graphite/epoxy, values of in-plane shear strength between 69 and 103 MPa (10 and 15 ksi) are typically

reported. The S_1 stress when damage initiates is large compared to these in-plane strengths. However, in-plane strengths of unidirectional material do not involve fiber failure as do the failures here.

Tests were conducted to determine a shear strength S_u that could be used with a maximum shear stress criterion to predict fiber failure. Using core drills, disks were cut from remnants of specimens from the cylinder [1-4]. See figure 10. Compression loads were applied to both faces of each disk, giving σ_{zz} stresses on the outer surface similar in nature to the contact stresses but more uniform. The diameters of the disks were 2.5, 3.8, and 5.1 cm (1.0, 1.5, and 2.0 in.). Several specimens with each diameter were crushed. The average compression strength was 620 MPa (90 ksi). The strength varied little with specimen diameter. The failure surfaces intersected the free edge at approximately a 45° angle, which is consistent with planes of principal shear stress. The failures involved fibers like those in the simulated impact tests. The principal shear stress at the free edge is $1/2$ the compression stress. For a uniform σ_{zz} , the shear strength is one-half the compression strength or 310 MPa (45 ksi). This value is considerably larger than the in-plane strengths of unidirectional material, and somewhat larger than S_1 when fiber damage initiated.

Contours of p_c/S_{\max} values are plotted in figure 11 using the normalized coordinates ρ and ζ , where S_{\max} is the maximum of the principal shear stresses. For $p_c/S_{\max} \leq 5$, $S_{\max} = S_1$; and, for $p_c/S_{\max} > 5$, $S_{\max} = S_1$ everywhere except $\rho \approx 0$ and $\zeta > 1$. For $S_{\max} = S_u$, the stress contours are equivalent to damage contours. The contours are approximately circular in cross section, giving a somewhat spherical damage region. Damage initiates below the surface at $\zeta = 0.482$ when the average contact pressure is $2.15 S_{\max}$. As the pressure increases, the contour moves radially outward much like a sound wave and reaches the surface for $p_c/S_{\max} \approx 5$.

The size of the damage contours in figure 11 are normalized by r_c . For a given value of p_c , r_c in equation (7) increases in proportion to indenter radius R_i . Thus, the size of the damage contours increase in proportion to R_i . It should be noted that Love's solution does not account for damage and is only valid in the strictest sense for predicting the onset of damage. Therefore, even if the FWC laminate were homogeneous and isotropic, the predictions of damage size with Love's solution would only be approximate.

The maximum depths of the damage contours in figure 11 ($\rho = 0$) were plotted against the average contact pressure in figure 12 for $S_1 = S_u = 310$ MPa (45 ksi). The depths were calculated with

$$\frac{4S_1}{3p_c} = \left(\frac{5}{2} - \nu_t\right)(1 + \zeta^2)^{-1} + (1 - \nu_t)\zeta^2(1 + \zeta^2)^{-1} + (1 + \nu_t)\zeta \tan^{-1}\left(\frac{1}{\zeta}\right) \quad (9)$$

A vertical line was drawn from the initiation depth to the abscissa. This line represents the pressure threshold for fiber damage. The depth ζ_0 where damage initiates is equal to the location of the maximum value of S_1 . Setting the derivative with respect to ζ of equation (9) to zero gives

$$0 = 3\zeta_0 - (1 + \nu_t)(1 + \zeta_0^2)[(1 + \zeta_0^2)\tan^{-1}\left(\frac{1}{\zeta_0}\right) - \zeta_0] \quad (10)$$

The maximum depths of fiber breaks for the deplied specimens are also plotted in figure 12 for comparison. The damage depth was normalized by the contact radius r_c calculated with equation (3) and $n_0 = 4.52$ GPa (656 ksi). As noted previously, r_c increases in proportion to R_i . Thus, r_c values for the 50.8-mm-diameter (2.0-in.) indenter are four times those for the 12.7-mm-diameter (0.5-in.) indenter. The filled symbols indicate visible surface damage, and the open symbols indicate no visible surface damage. The 5.08-cm-diameter (2.0-in.) indenter made no visible surface damage for average contact pressures below 590 MPa (86 ksi). The pressures to cause visible damage were a little larger for the smaller indenters. Considering the wide range of r_c values, the normalized damage depths coalesce fairly well for the various indenter diameters, indicating that damage depth is proportional to the contact radius as predicted. Equation (9) with $S_u = 310$ MPa (45 ksi) gives a lower bound on the measured damage depths. The predictions were very good considering Love's solution was for a homogeneous isotropic body and did not account for damage. Equation (9) with $S_u = 228$ MPa (33 ksi) is also plotted in figure 12 to indicate an upper bound on damage for the test data. This curve also represents the threshold for damage initiation quite well.

The sensitivity of the results to the contact pressure distribution was also determined. For uniform contact pressure [8], the shear stress is also maximum for $\rho = 0$ and is given by

$$\frac{2S_1}{p_c} = \frac{1}{2} - \nu_z + \left(\nu_t - \frac{1}{2}\right)\zeta(1 + \zeta^2)^{-1/2} + \frac{3}{2}\zeta(1 + \zeta^2)^{-3/2} \quad (11)$$

The value of ζ for maximum S_1 is given by

$$\zeta_0^2 = \frac{(1 + \nu_t)}{\left(\frac{7}{2} - \nu_t\right)} \quad (12)$$

Equation (11) with $S_1 = S_u = 310$ MPa (45 ksi) was also plotted in figure 12. For a given value of p_c ; the damage depths are much larger for varying pressure than for uniform pressure.

The maximum width of the damage contours in figure 11 are plotted against p_c in figure 13 for values of $S_1 = S_u = 228$ and 310 MPa (33 and 45 ksi). The maximum half-crack lengths for the deplied specimens are plotted for comparison. When a layer contained more than one crack, the length of the longest was plotted. Both predictions and measurements are normalized by contact radius as before. In this case, the curves for $S_u = 228$ and 310 MPa (33 and 45 ksi) are a little too low to be an upper and lower bound, respectively, on crack length.

The predicted and measured values of maximum half-crack length in figure 13 were divided by the maximum values of damage depth in figure 12 and plotted in figure 14. As contact pressure increases beyond the threshold for damage initiation, the predicted ratios quickly increase from zero to 0.87 and then gradually descend. A representative value is about 0.8 for pressures up to 1 GPa (145 ksi). On the other hand, the measured values vary from 0.9 to 1.5. Notice that reducing the shear strength S_u reduces the threshold for damage initiation but has no significant affect on the aspect ratio. Thus, the strength S_u cannot be adjusted to represent the crack lengths. A method to predict tension strength after impact using surface flaw analysis was proposed [1-4]. The depth and aspect ratio of an equivalent surface flaw was assumed to be equal to the predicted depth and aspect ratio in figures 12 and 14. Since strength decreases with increasing values of the aspect ratio, the use of the predicted aspect ratios in figure 14 will give strengths that are too large. One could improve the accuracy of strength predictions by using the predicted depth and a constant aspect ratio between 0.9 to 1.5

The measured damage contours in figure 7 were normalized by contact radii and plotted in figure 15. The values of radii were calculated as before. Contours were predicted for the upper bound value of $S_u = 228$ MPa (33 ksi) and plotted for comparison. Except for a pressure of 514 MPa (74.5 ksi), the measured and predicted contours are in reasonably good agreement. For 514 MPa (74.5 ksi), the measured damage contours for the 1.27- and 2.54-cm-diameter (0.5- and 1.0-in.) indenters are considerably greater than predicted. Also, the predicted damage contours do not reach the surface, whereas the measured ones do. In all of the specimens tested and deplied in the present study, the fiber breaks never first appeared below the surface as predicted. Sometimes intermediate layers were without fiber breaks, but never the surface layer. In fact, as noted previously, the layers near the surface often contained multiple cracks. As suggested previously, the large compressive stresses near the surface may have caused compressive failures there first. Also, the heterogeneous or layered nature of the laminate may cause Love's solution to be more incorrect near the surface than below the surface.

Finally, observations of visible surface damage are presented in a bar chart in figure 16. For each contact pressure and indenter diameter, the surface damage is described as barely visible or readily visible. Readily visible damage would likely be detected in a careful, methodical inspection. Barely visible damage was a slight indentation that could be felt more easily than seen. It would only be detected if the impact site were known. The data indicate that the minimum pressure to cause barely visible surface damage (permanent indentation) and actual fiber damage are nearly the same. For a given pressure, the damage is more visible for a larger indenter than a smaller

indenter. The difficulty in seeing the damage caused by a small indenter is primarily due to the small contact diameter and hence the small damage size. For example, at a pressure of 514 MPa (74.6 ksi), equation (5) gives contact diameters of 4.5, 9.0, and 18.1 mm (0.18, 0.35, and 0.71 in.) for the 1.27-, 2.54-, and 5.08-cm-diameter (0.5-, 1.0-, and 2.0-in.) indenters, respectively. Also, it can be shown that the indentation depth increases with increasing indenter diameter for a given contact pressure.

It should be noted that, although damage is less visible for smaller indenter radii for a given contact pressure, the converse is true for impacts with a given kinetic energy and mass [1]. For the impacts, contact pressures were much larger for smaller indenter radii and hence the craters were deeper and more visible. Although the impact damage was much less visible for larger radii, residual tension strengths were reduced about as much as those for the smaller radii. Thus, impacts are actually more critical with regard to detection for larger indenter radii than for smaller radii.

CONCLUSIONS

A study was made to determine the extent of fiber damage caused by low-velocity impact of spherical impacters to a very thick graphite/epoxy laminate. The laminate was cut from a filament wound case (FWC) being developed for the solid rocket motors of the Space Shuttle. The case was wound using a wet process with AS4W graphite fiber and HBRF-55A epoxy. Impacts were simulated under quasi-static conditions by pressing hemispherically shaped indenters against the laminate at different locations. The contact force and indenter diameter were varied from location to location. The forces were chosen for each indenter diameter to produce contact pressures below and above that required to initiate damage. After the forces were applied, the laminate was cut into smaller pieces so that each piece contained a test site. Then the pieces were deplieed and the individual plies were examined to determine the extent of fiber damage. Broken fibers were found in the outer layers directly beneath the contact site. The locus of broken fibers in each layer resembled a crack normal to the direction of the fibers. The maximum length and depth of the cracks increased with increasing contact pressure and indenter diameter. The cracks initiated at a critical value of average contact pressure between 408 and 514 MPa (59.2 and 74.6 ksi) for each indenter diameter. Residual craters accompanied the onset of damage. However, the residual craters were small and not readily visible (detectable) for pressures less than 589 to 698 MPa (85.4 to 101 ksi), depending on indenter diameter. The smaller indenters made smaller craters for a given pressure.

The internal stresses in the laminate were calculated using Hertz's law and Love's solution for pressure applied on part of the boundary of a semi-infinite body. The maximum length and depth of the cracks were predicted using a maximum shear stress criterion. The predictions and measurements were in good agreement. A shear strength of 310 MPa (45 ksi), determined by a compression test, gave a lower bound to the damage depth. A value of 228 MPa (33 ksi) gave an upper bound with good agreement for damage initiation. The analysis underpredicted the crack lengths somewhat.

ACKNOWLEDGMENTS

Mr. Mickey R. Gardner, a Langley Research Center engineering technician, performed the laboratory work. He was assisted in deplying the specimens by Ann E. Davis, a participant in the Summer High School Apprenticeship Research Program.

REFERENCES

1. Poe, Jr., C. C.; Illg, W.; and Garber, D. P.: A Program to Determine the Effect of Low-velocity Impacts on the Strength of the Filament-wound Rocket Motor Case for the Space Shuttle. NASA TM-87588, September 1985.
2. Poe, Jr., C. C.; Illg, W.; and Garber, D. P.: Tension Strength of a Thick Graphite/epoxy Laminate after Impact by a 1/2-In.-Radius Impacter. NASA TM-87771, July 1986.
3. Poe, Jr., C. C.; Illg, W.; and Garber, D. P.: Strength of a Thick Graphite/epoxy Laminate after Impact by a Blunt Object. NASA TM-89099, February 1987.
4. Poe, Jr., C. C.; and Illg, W.: Tensile Strength of a Thick Graphite/Epoxy Rocket Motor Case After Impact by a Blunt Object. 1987 JANNAF Composite Motor Case Subcommittee Meeting, CPIA Publication 460, Feb. 1987, pp. 179-202.
5. Freeman, S. M.: Characterization of Lamina and Interlaminar Damage in Graphite/Epoxy Composites by the Deply Technique. Composite Materials: Testing and Design (Sixth Conference), ASTM STP 787, 1982, pp. 50-62.
6. Greszczuk, Longin B.: Damage in Composite Materials due to Low Velocity Impact. Impact Dynamics, John Wiley & Sons, Inc., 1982, pp. 55-94.
7. Tan, T. M.; and Sun, C. T.: Use of Statical Indentation Laws in the Impact Analysis of Laminated Composite Plates. Transactions of the ASME, Vol. 52, March 1985, pp.6-12.
8. Love, A. E. H.: The Stress Produced in a Semi-infinite Solid by Pressure on Part of the Boundary. Phil. Trans. Roy. Soc. Lond. Series A, vol. 228, 1929, pp. 377-420

Table 1. Contact forces and pressures for the various indenters.

Contact pressure, MPa (ksi)	Contact force, kN (kip) for indenter diameters of -		
	1.27 cm (0.50 in.)	2.54 cm (1.00 in.)	5.08 cm (2.00 in.)
408 (59.2)	4.18 (0.94)	16.6 (3.74)	66.7 (15.0)
514 (74.6)	8.36 (1.88)	33.3 (7.48)	133. (30.0)
589 (85.4)	12.5 (2.82)	49.8 (11.2)	200. (45.0)
648 (94.0)	16.7 (3.76)	66.7 (15.0)	267. (60.0)
698 (101.)	20.9 (4.70)	83.2 (18.7)	334. (75.0)
742 (108.)	25.1 (5.64)	99.6 (22.4)	400. (90.0)

a Contact pressures greater than 640 MPa (93 ksi) caused readily visible craters for 2.54-cm-diameter (1.0-in.) indenter [2-4].

Table II. Indenter diameter, contact force, fiber damage size, and visibility of surface damage.

Specimen number	Indenter diameter, mm (in.)	Contact force, kN (kip)	Maximum crack length, mm (in.)	Maximum crack depth, mm (in.)	Visibility of surface damage
1-19	12.7 (0.50)	4.18 (0.94)	0.0	0.0	N
1-22		8.36 (1.88)	3.2 (.13)	1.3 (.05)	B
1-25		12.5 (2.82)	5.1 (.20)	2.6 (.10)	B
1-28		16.7 (3.76)	6.4 (.25)	2.1 (.08)	B
1-31		20.9 (4.70)	5.1 (.20)	2.8 (.11)	R
1-34		25.1 (5.64)	7.6 (.30)	2.8 (.11)	R
1-20	25.4 (1.00)	16.6 (3.74)	0.0	0.0	N
1-23		33.3 (7.48)	7.6 (.30)	5.0 (.20)	B
1-26		49.8 (11.2)	7.6 (.30)	1.7 (.07)	B
1-29		66.7 (15.0)	10.2 (.40)	3.6 (.14)	R
1-32		83.2 (18.7)	-	-	R
1-35		99.6 (22.4)	12.7 (.50)	5.4 (.21)	R
1-17		99.6 (22.4)	10.2 (.40)	5.6 (.22)	R
1-21	50.8 (2.00)	66.7 (15.0)	0.0	0.0	N
1-24		133. (30.0)	8.9 (.35)	2.8 (.11)	B
1-27		200. (45.0)	17.8 (.70)	9.0 (.35)	R
1-30		267. (60.0)	20.3 (.80)	10.1 (.40)	R
1-33		334. (75.0)	25.4 (1.00)	9.4 (.37)	R
1-36		400. (90.0)	27.9 (1.10)	14.8 (.58)	R
1-18		400. (90.0)	25.4 (1.00)	12.7 (.50)	R

N - nonvisible.

B - barely visible.

R - readily visible.

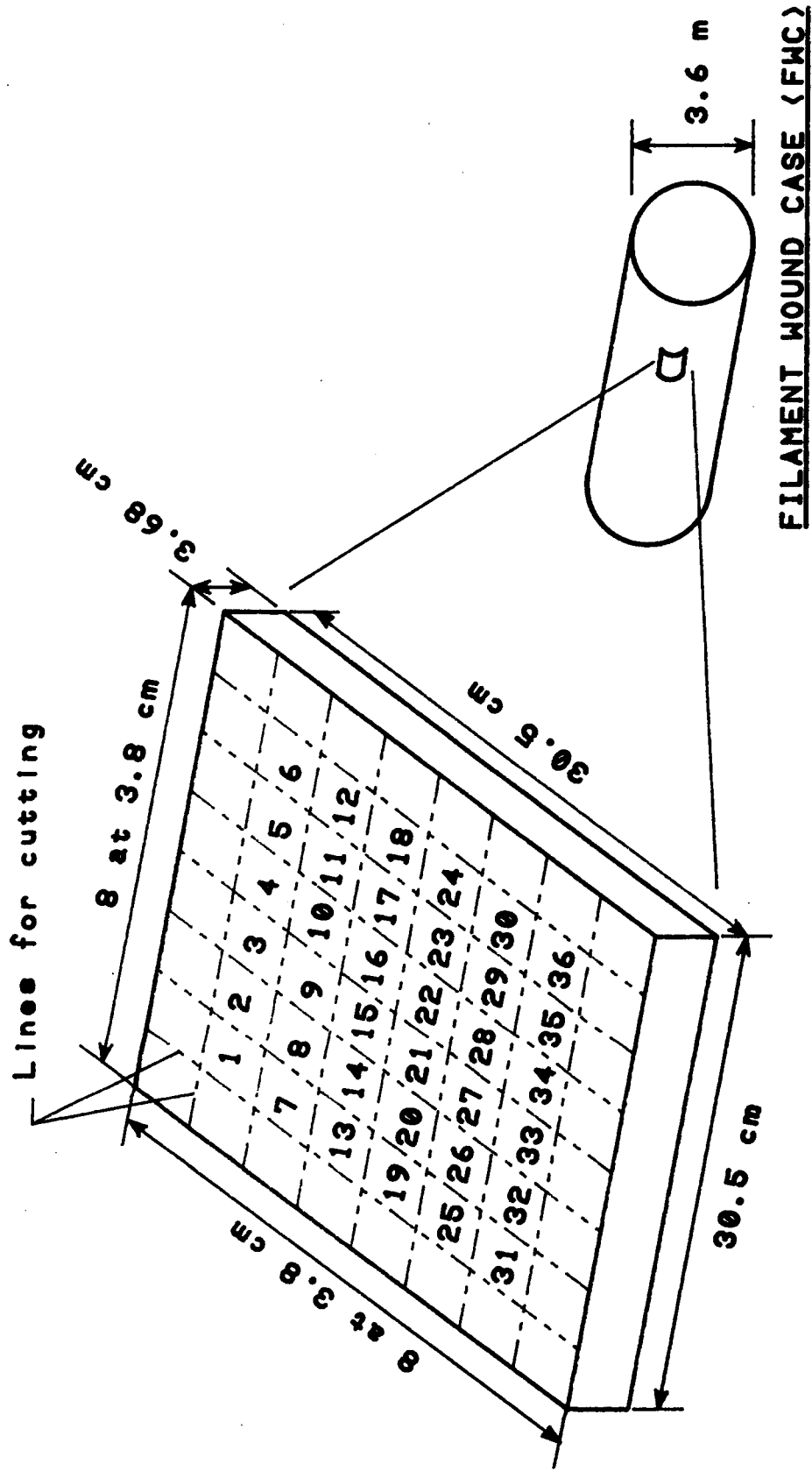


Figure 1.- Specimen layout.

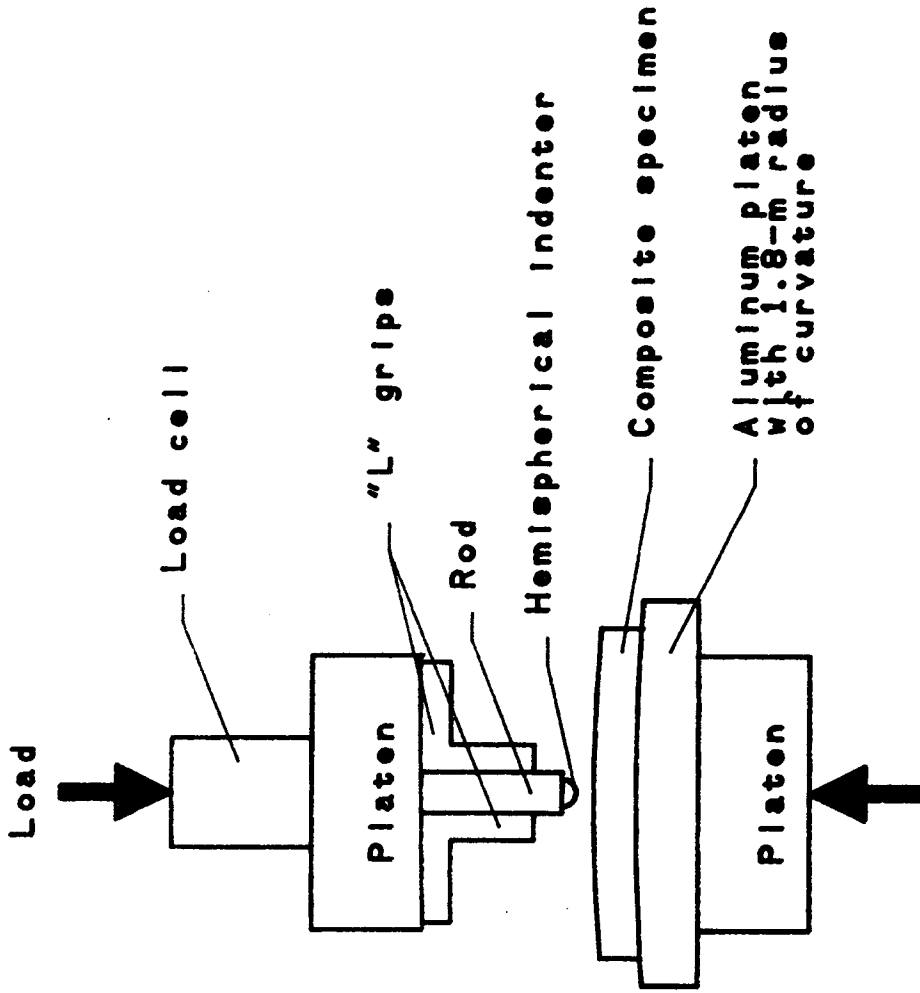
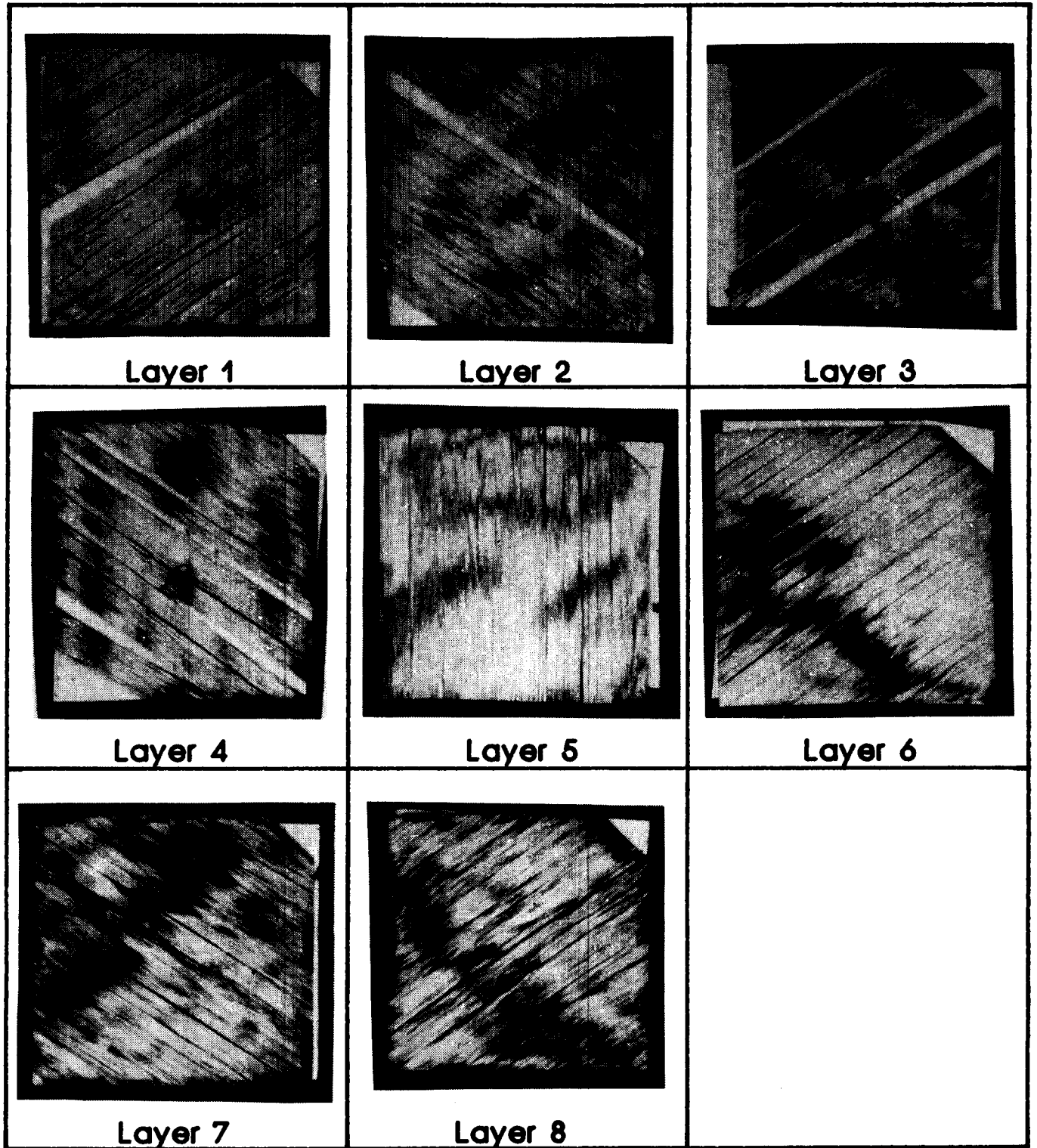


Figure 2.- Test apparatus.



**Figure 3. Photographs of damaged layers from Specimen 1-28
(127-cm-dia. indenter and 16.7-kN contact force).**

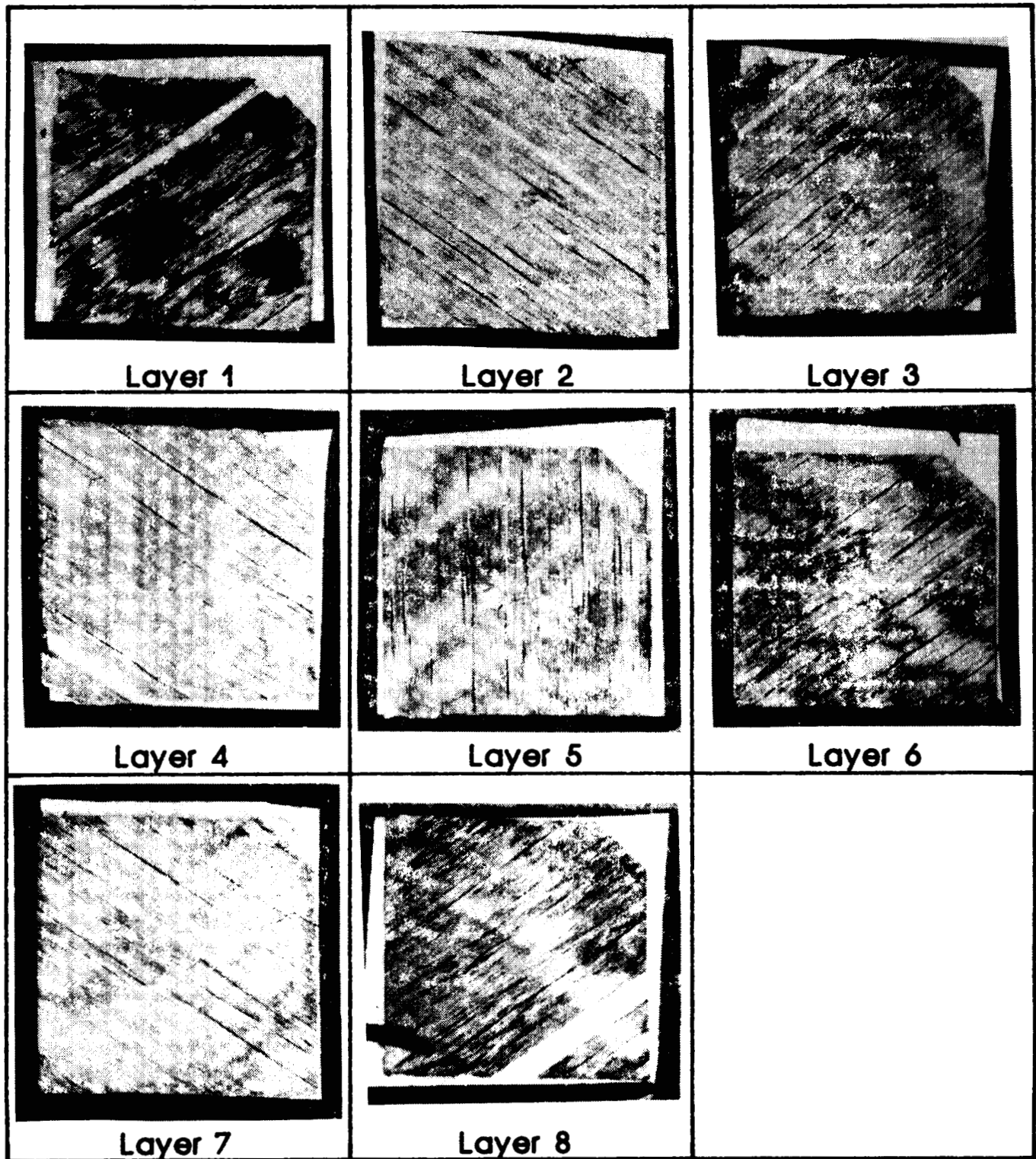
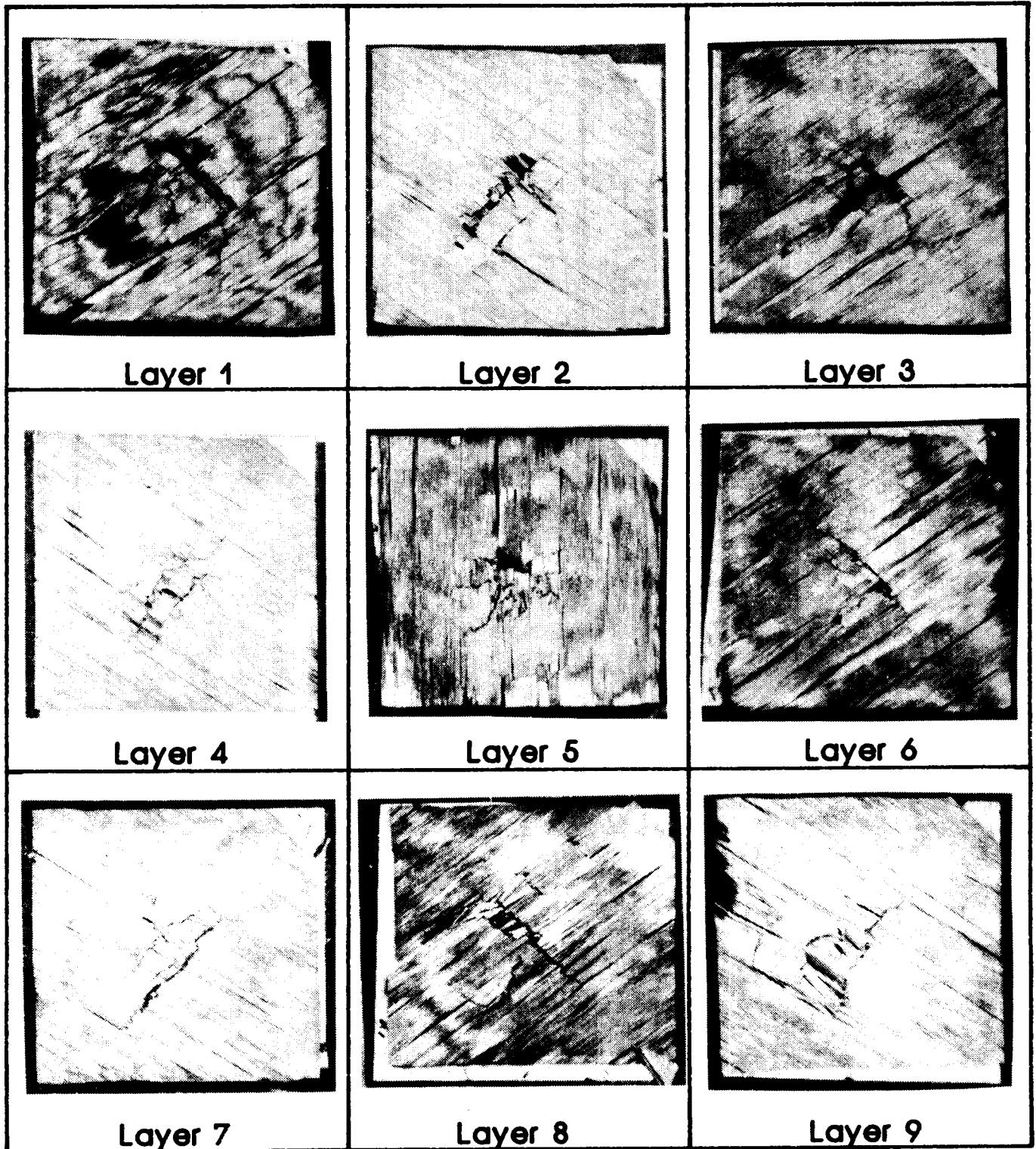
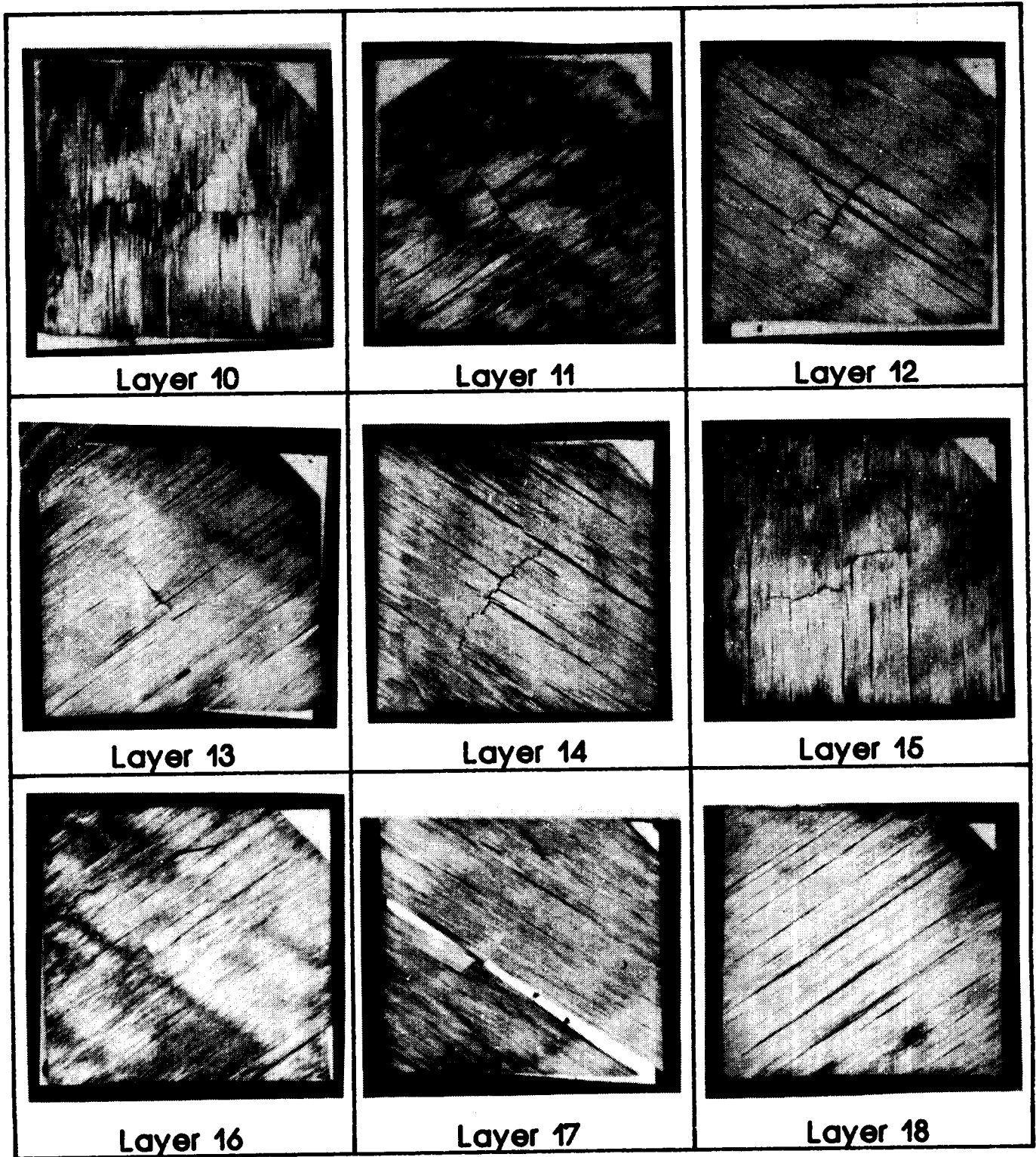


Figure 4. Photographs of damaged layers from Specimen 1-29
(2.54-cm-dia. indenter and 66.7-kN contact force).



(a) Layers 1 through 9.

Figure 5. Photographs of damaged layers from Specimen 1-30
(6.08-cm-dia. indenter and 267-kN contact force).



(b) Layers 10 through 18.

Figure 5. Concluded.

ORIGINAL PAGE IS
OF POOR QUALITY

ORIGINAL PAGE IS
OF POOR QUALITY

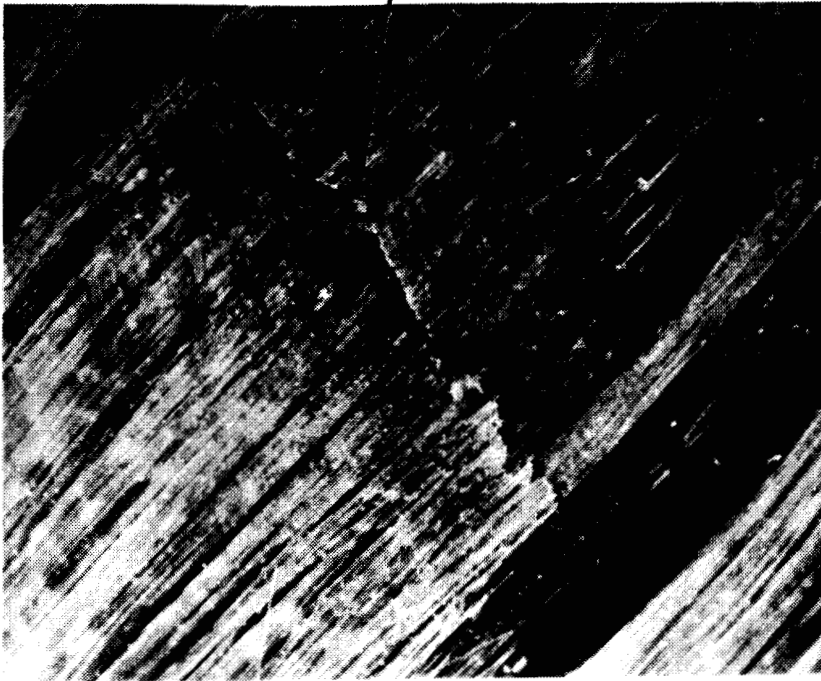
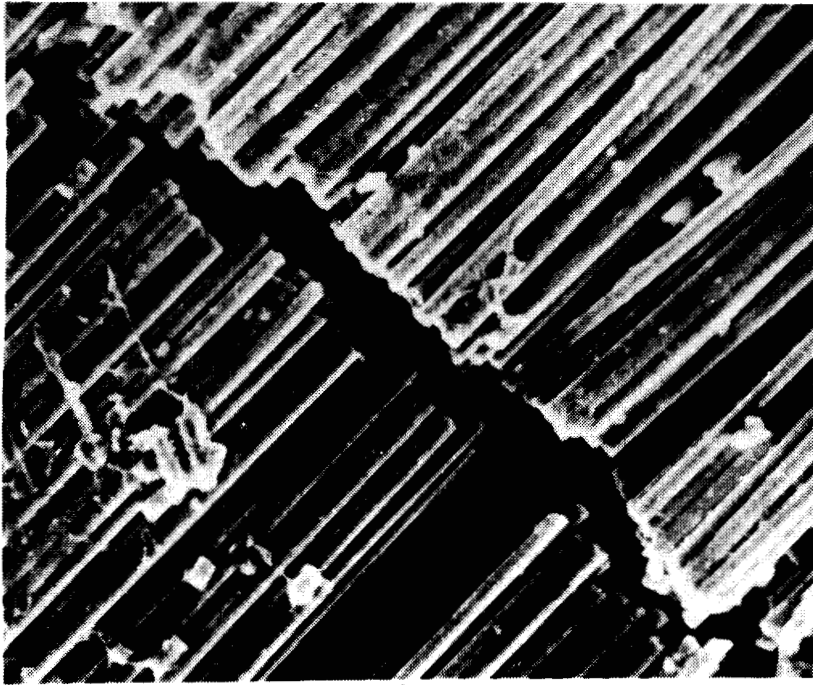


Figure 6. Photomicrographs of fibers broken by impact (ayer 7, the deepest with damage.)

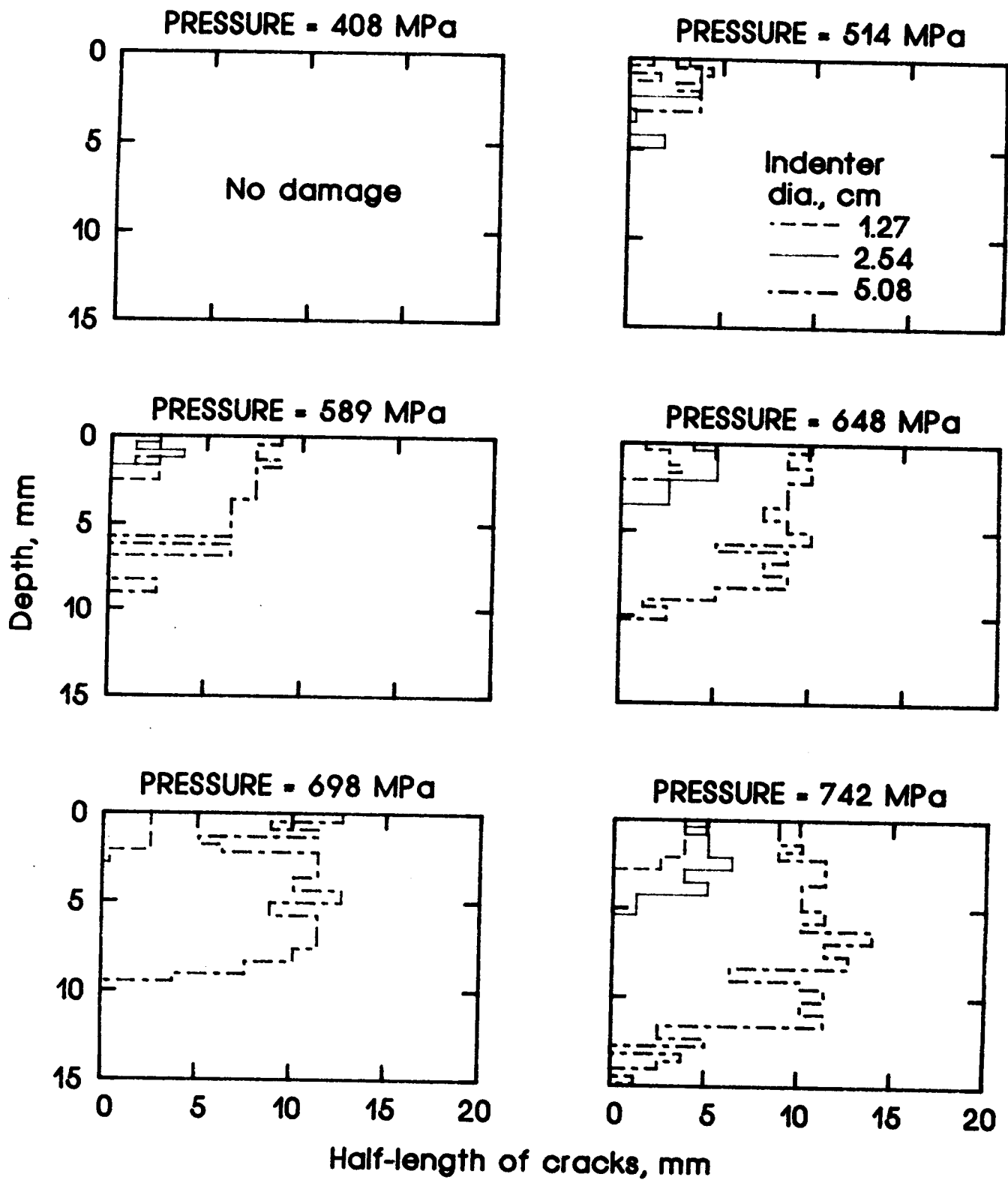


Figure 7. Fiber damage contours from deploded specimens for various average contact pressures.

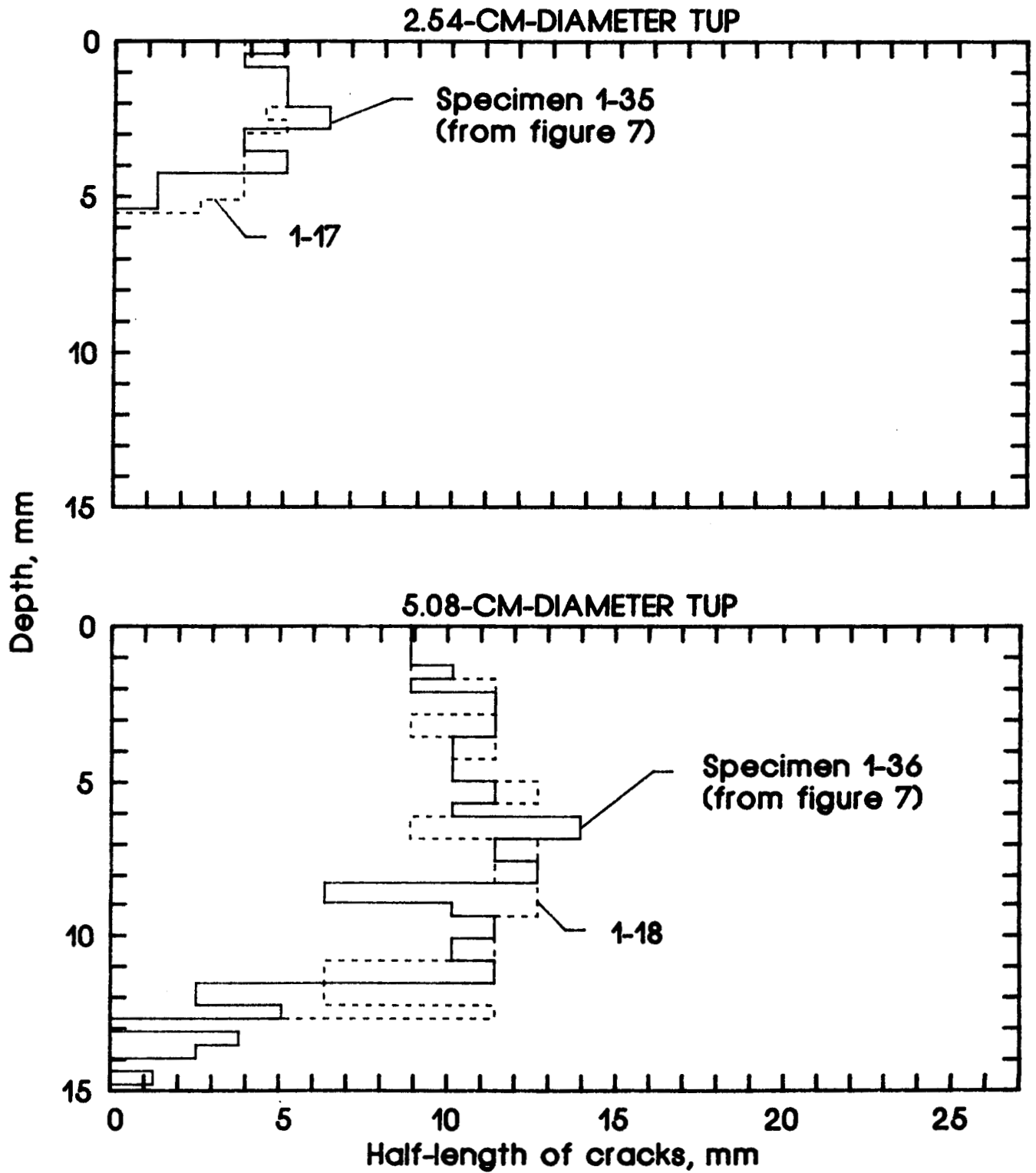


Figure 8. Fiber damage contours from deplied specimens for replicate tests with an average contact pressure of 742 MPa.

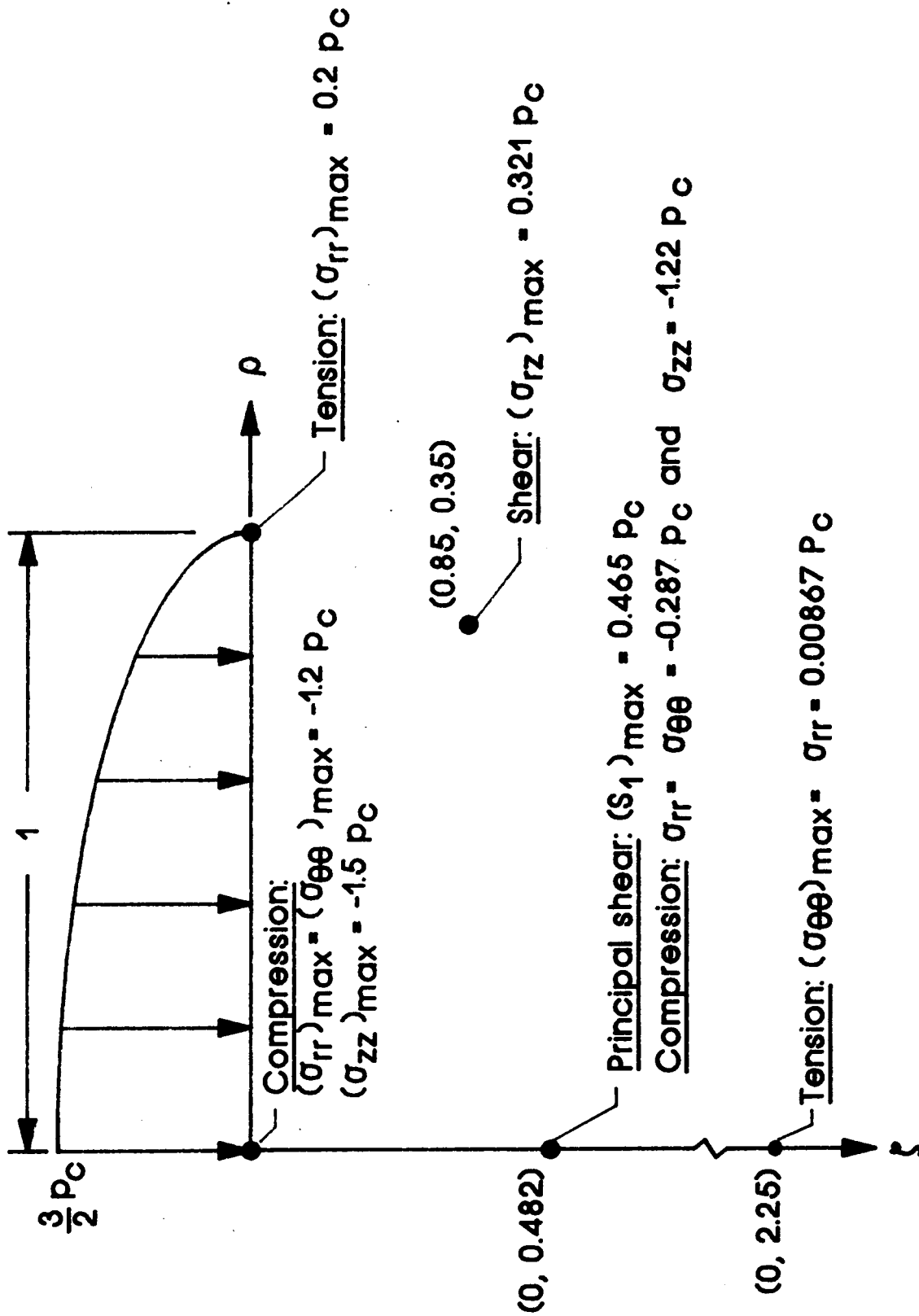


Figure 9. Maximum values of stress in cylindrical coordinates from Love's solution with Poisson's ratio = 0.3.

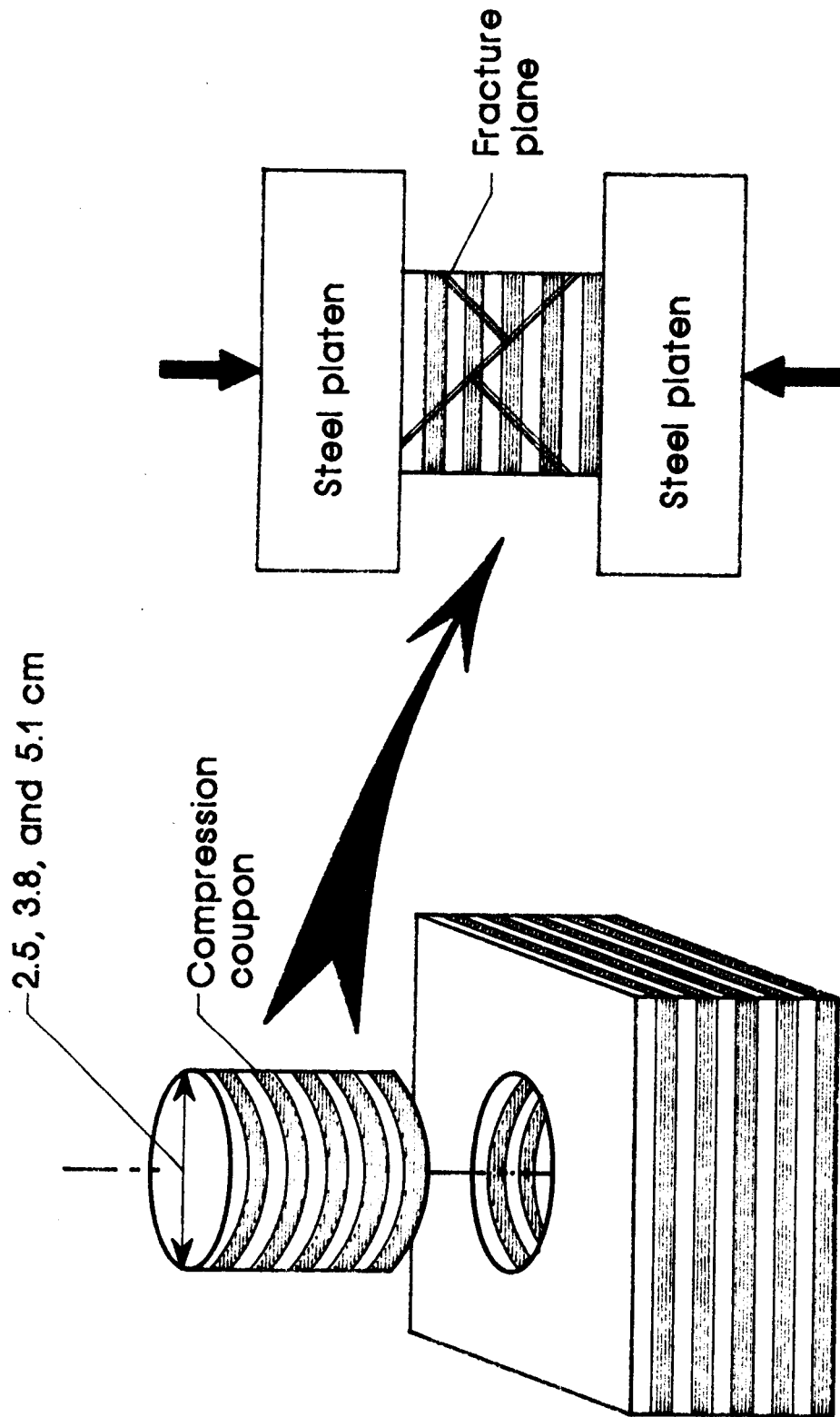


Figure 10.- Compression test for shear strength.

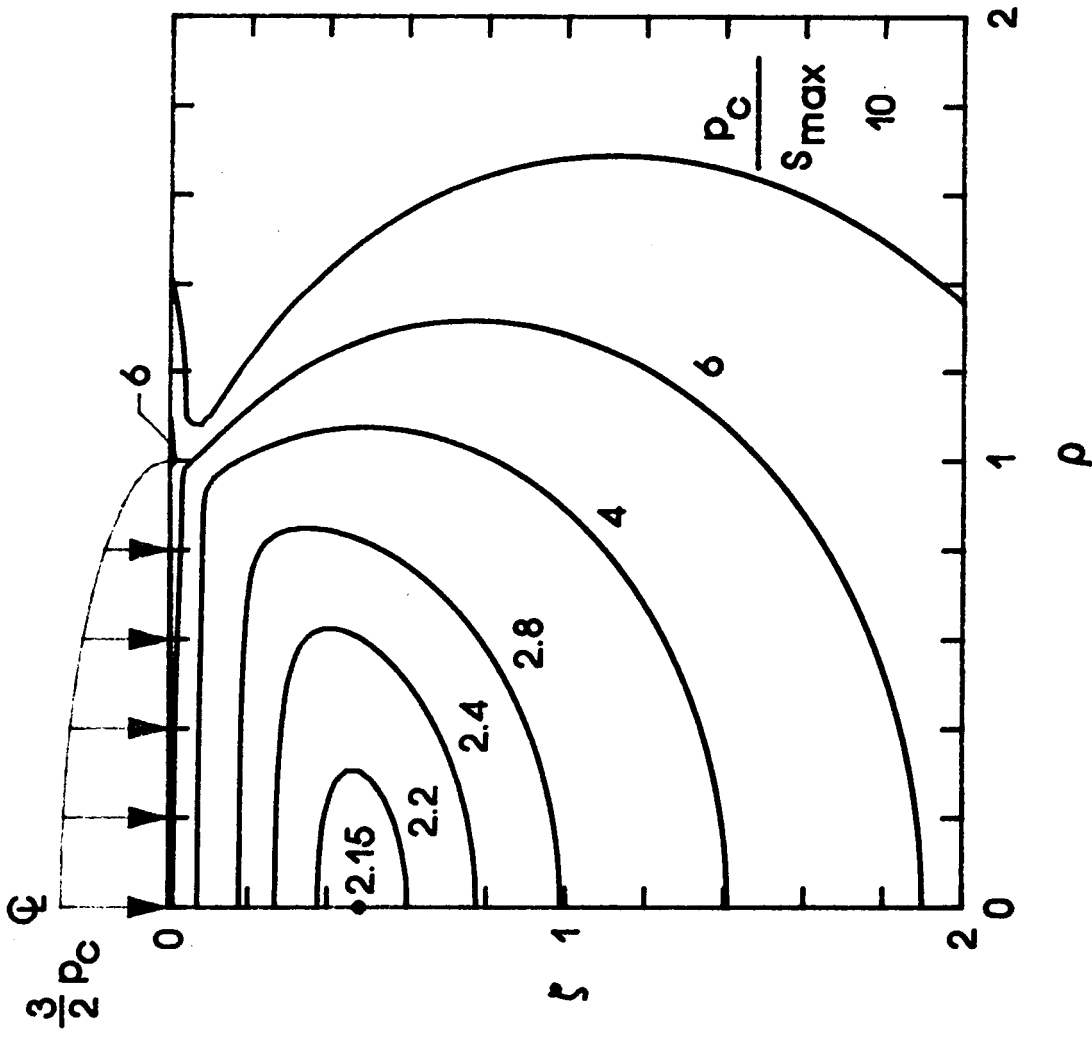


Figure 11- Maximum shear stress contours according to Love's solution (Poisson's ratio = 0.3).

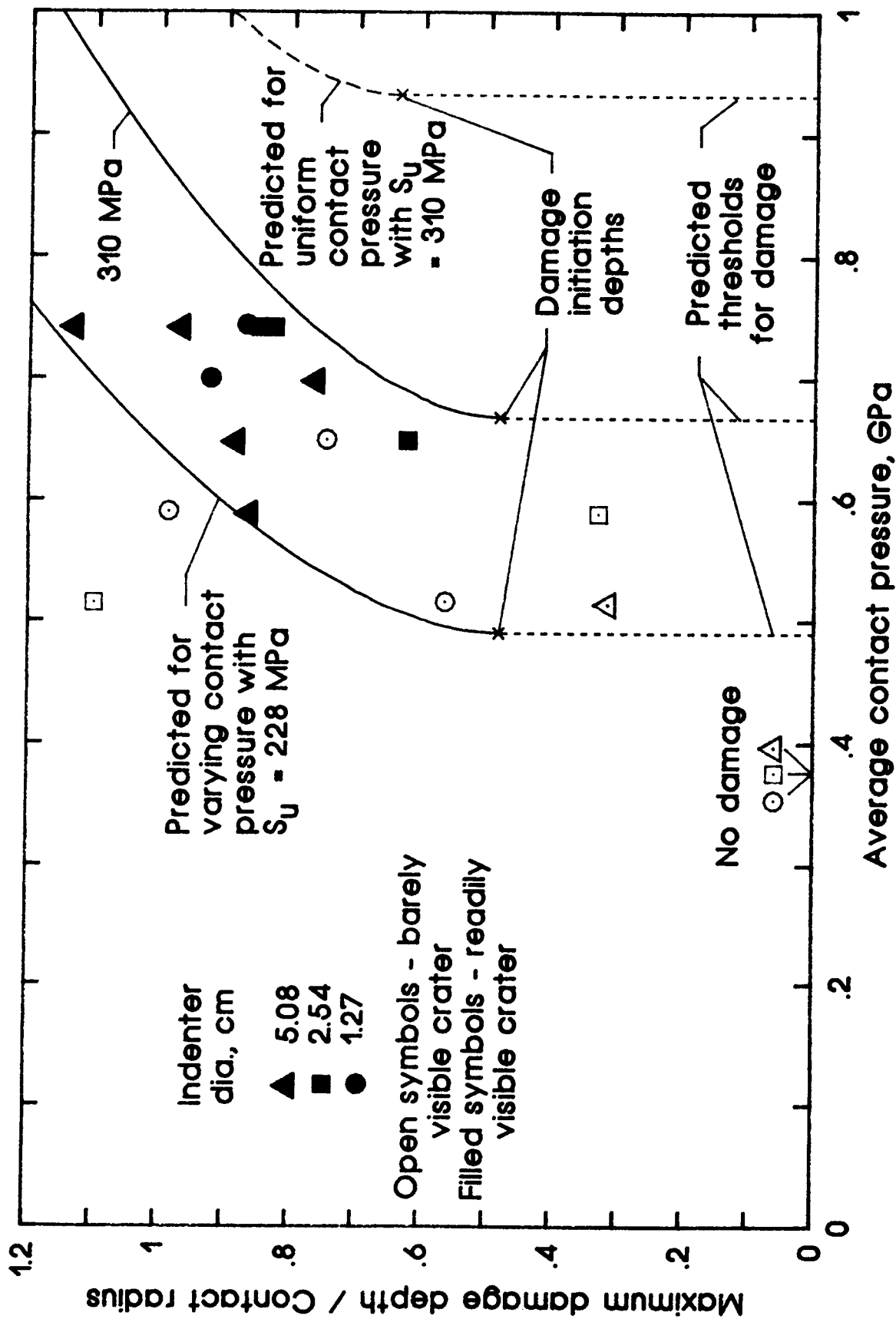


Figure 12. Comparison of predicted and measured damage depth.

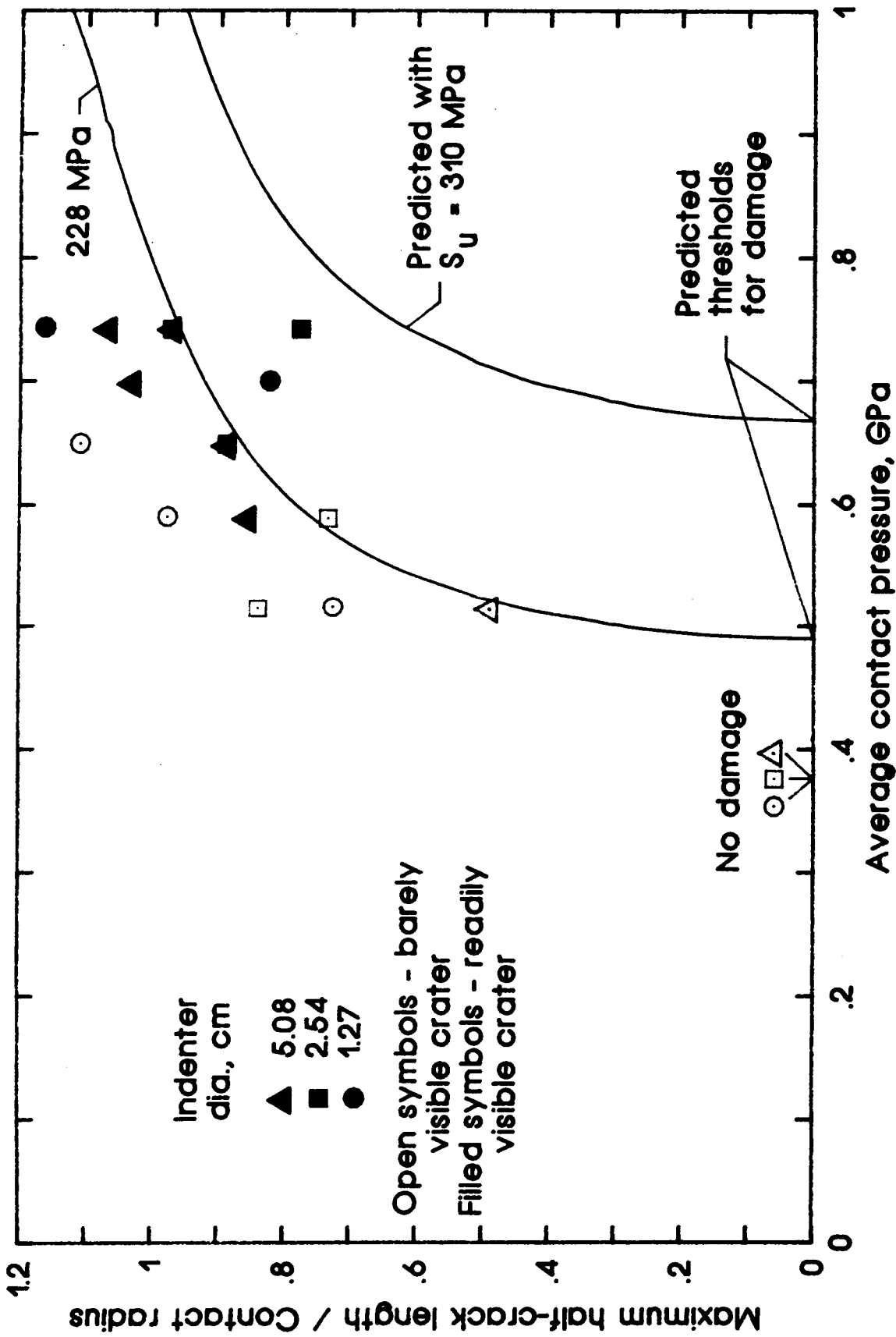


Figure 13. Comparison of predicted and measured crack length.

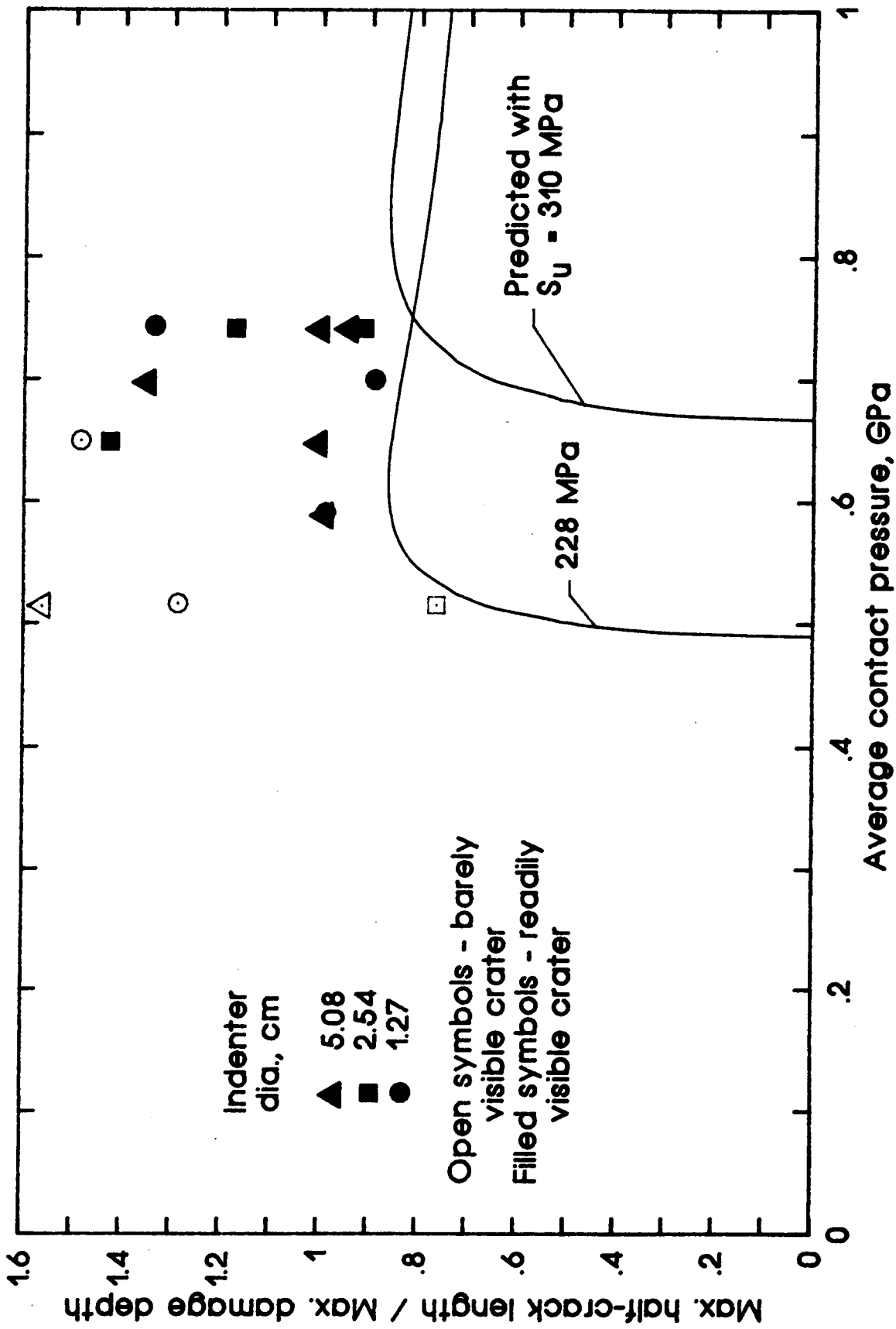


Figure 14. Comparison of predicted and measured aspect ratios of damage.

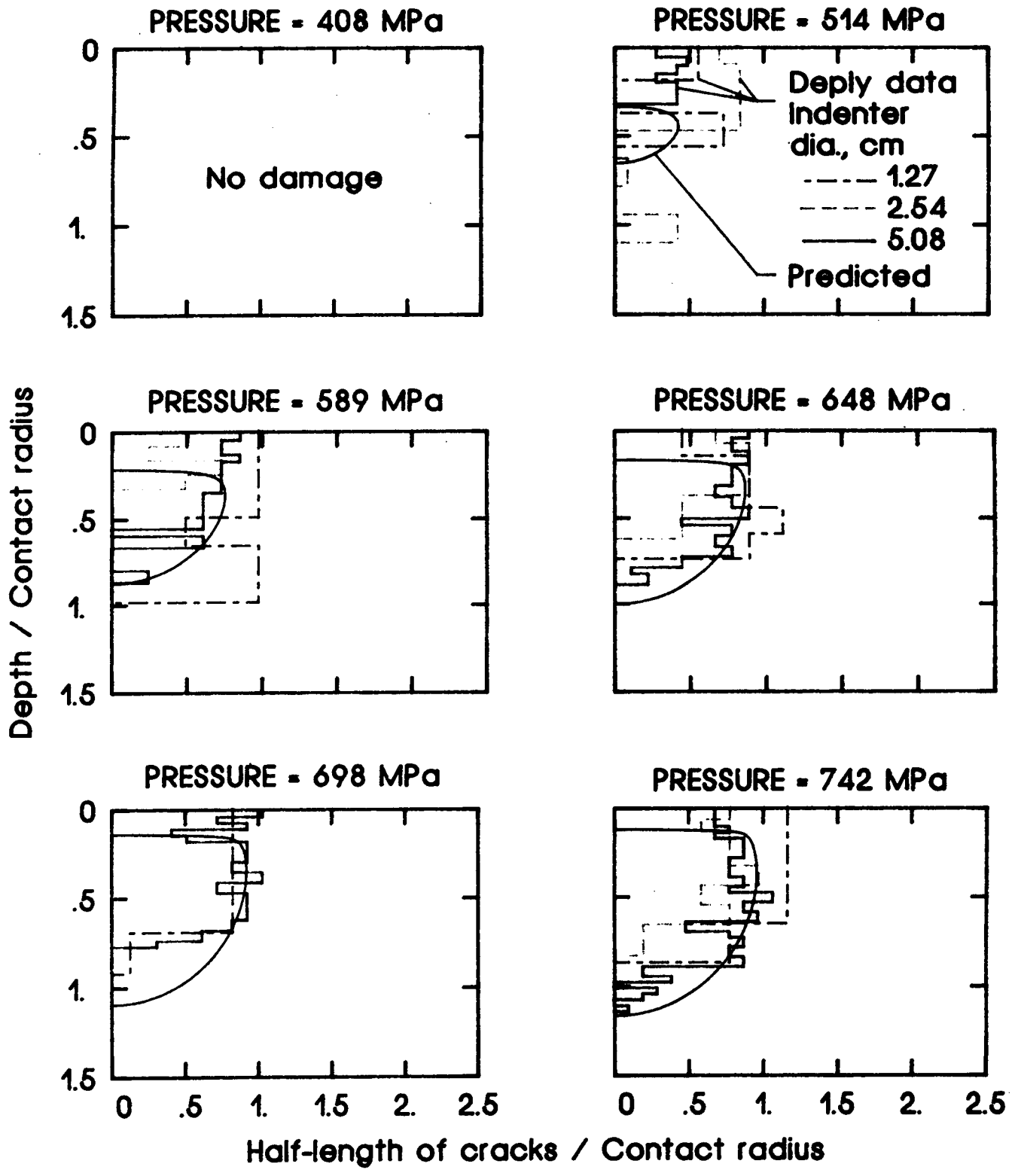


Figure 15. Comparison of predicted ($S_u = 228$ MPa) and measured damage contours for various average contact pressures.

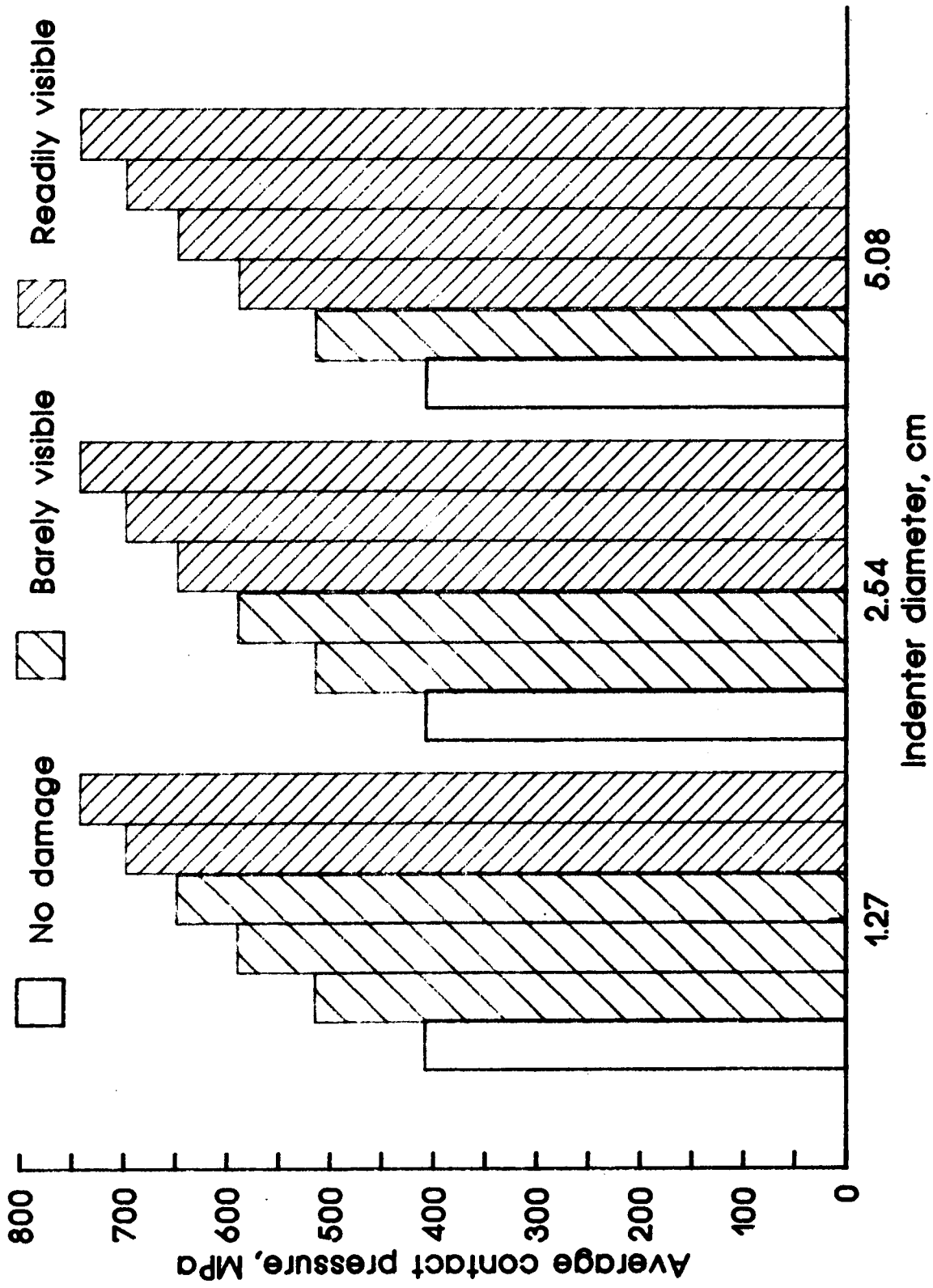


Figure 16.- Visibility of surface damage.

Standard Bibliographic Page

1. Report No. NASA TM-100539		2. Government Accession No.		3. Recipient's Catalog No.	
4. Title and Subtitle Simulated Impact Damage in a Thick Graphite/Epoxy Laminate Using Spherical Indenters				5. Report Date January 1988	
				6. Performing Organization Code	
7. Author(s) C. C. Poe, Jr.				8. Performing Organization Report No.	
				10. Work Unit No. 506-43-11-04	
9. Performing Organization Name and Address NASA Langley Research Center Hampton, VA 23665-5225				11. Contract or Grant No.	
				13. Type of Report and Period Covered Technical Memorandum	
12. Sponsoring Agency Name and Address National Aeronautics and Space Administration Washington, DC 20546				14. Sponsoring Agency Code	
				15. Supplementary Notes	
16. Abstract A study was made to determine the extent of fiber damage caused by low-velocity impact of spherical impacters to a very thick graphite/epoxy laminate. The laminate was cut from a filament wound case (FWC) being developed for the solid rocket motors of the Space Shuttle. The case was wound using a wet process with AS4W graphite fiber and HBRF-55A epoxy. Impacts were simulated under quasi-static conditions by pressing hemispherically shaped indenters against the laminate at different locations. The contact force and indenter diameter were varied from location to location. The forces were chosen for each indenter diameter to produce contact pressures below and above that required to initiate damage. After the forces were applied, the laminate was cut into smaller pieces so that each piece contained a test site. Then the pieces were deplied and the individual plies were examined to determine the extent of fiber damage. Broken fibers were found in the outer layers directly beneath the contact site. The locus of broken fibers in each layer resembled a crack normal to the direction of the fibers. The maximum length and depth of the cracks increased with increasing contact pressure and indenter diameter. The internal stresses in the laminate were calculated using Hertz's law and Love's solution for pressure applied on part of the boundary of a semi-infinite body. The maximum length and depth of the cracks were predicted using a maximum shear stress criterion. The predictions and measurements were in good agreement.					
17. Key Words (Suggested by Authors(s)) Graphite/epoxy Composite Filament-winding Motor case Impact damage Contact pressure			18. Distribution Statement Unclassified - Unlimited Subject Category - 24		
19. Security Classif.(of this report) Unclassified		20. Security Classif.(of this page) Unclassified		21. No. of Pages 34	22. Price A03

For sale by the National Technical Information Service, Springfield, Virginia 22161